Review of Scientific Instruments

Design and testing of drift free force probe experiments with absolute distance control

Cite as: Rev. Sci. Instrum. **93**, 073705 (2022); https://doi.org/10.1063/5.0083834
Submitted: 30 December 2021 • Accepted: 12 June 2022 • Published Online: 12 July 2022

Kai A. Schwenzfeier and Markus Valtiner

View Online Export Citation CrossMark

ARTICLES YOU MAY BE INTERESTED IN

A cryogenic torsion balance using a liquid-cryogen free, ultra-low vibration cryostat
Review of Scientific Instruments **93**, 064505 (2022); https://doi.org/10.1063/5.0089933

Construction of a vector-field cryogenic magnetic force microscope
Review of Scientific Instruments **93**, 063701 (2022); https://doi.org/10.1063/5.0092264

PIONEER, a high-resolution single-crystal polarized neutron diffractometer
Review of Scientific Instruments **93**, 073901 (2022); https://doi.org/10.1063/5.0089524

Read Now!
Review of Scientific Instruments
Special Issue: Advances in Measurements and Instrumentation Leveraging Embedded Systems

AIP Publishing

© 2022 Author(s).

Review of Scientific Instruments ARTICLE scitation.org/journal/rsi

Design and testing of drift free force probe experiments with absolute distance control

Cite as: Rev. Sci. Instrum. 93, 073705 (2022); doi: 10.1063/5.0083834
Submitted: 30 December 2021 • Accepted: 12 June 2022 •
Published Online: 12 July 2022

View Online Export Citation CrossMark

Kai A. Schwenzfeier and Markus Valtiner[a)]

AFFILIATIONS

Applied Interface Physics, Department of Applied Physics, Vienna University of Technology, Wiedner Hauptstraße 8-10, A-1040 Vienna, Austria

[a)]Author to whom correspondence should be addressed: valtiner@iap.tuwien.ac.at

ABSTRACT

After almost 35 years of truly successful and transformative advancements, Atomic Force Microscopy (AFM) and, in general, scanning probe microscopy still have a fundamental limitation. This is constant drift and uncontrolled motion of probe and tested surface structures with respect to each other. This is inherently linked to the currently accepted design principle—only forces are measured, and distances are inferred from force measurements and piezo motions. Here, we demonstrate and test a new setup, which combines advantages of AFM and the surface forces apparatus, where absolute distances are measured by Multiple Beam White Light Interferometry (MBI). The novel and unique aspect of this apparatus consists of a synergistic combination of white light interferometric measurement of the absolute distance by direct reflection from an AFM cantilever and a fast distance clamping and drift correction using an IR-laser Fabry–Pérot interferometry-based approach (FPI). We demonstrate the capabilities of the system by force/distance measurements, benchmarking of distance control by direct comparison of MBI and FPI, and discuss potential applications of the system. This novel setup has the potential to form, monitor, and stress a single molecule or ligand/receptor bond on the molecular hook with sub-nanometer control of molecular distances over in principle infinite times.

© 2022 Author(s). All article content, except where otherwise noted, is licensed under a Creative Commons Attribution (CC BY) license (http://creativecommons.org/licenses/by/4.0/). https://doi.org/10.1063/5.0083834

I. INTRODUCTION

Current Scanning Probe Microscopy (SPM) technology does not provide an ultra-stable 3D-reference frame to position an SPM probe with sub-Å resolution. In particular, Atomic Force Microscopy (AFM) does not provide a direct, simultaneous yet decoupled measure of forces and absolute position between the probe and a given point of interest (e.g., a single molecule) at a surface/interface. In current technology, the relative distance is inferred from the measured (or calibrated) displacement of the piezoelectric translation of the AFM probe or sample stage and the response of the cantilever spring.[1] Hence, an apparent distance is obtained by *a posteriori* interpretation of the ensuing force-vs-displacement characteristics and not through an independent method. Ensuing forces are measured as a function of the displacement of a piezoelectric translator, which is then converted into an apparent distance. The displacement of the piezoelectric translator is, however, not absolute with respect to a sample and is corrupted by uncontrolled mechanical and thermal drift of the whole microscope. This limits the time scale for controlled measurements at a given distance, during contactless hovering above a surface, to a few seconds (where drift is still insignificant). System drifts cannot be compensated *operando* by direct measurement. This limits AFM to processes that appear on short timescales (s). AFM force studies and therewith a large number of applications of AFM in biological and nano-sciences will benefit from a truly distance controlled AFM technology.

In the last few years, these fundamental design flaws of AFM have been increasingly realized across interdisciplinary fields. Current concepts resolve these issues at the expense of sensitivity and range. For instance, optical trapping in a backscattering geometry was used to provide accurate positioning of an AFM probe above a surface in 3D, yet limited to transparent substrate[2] static measurements. Likewise, absolute sample separation was measured between an AFM probe and a solid substrate in (and limited to) the presence of an irreversibly adsorbed film by analyzing a scattered evanescent wave that is generated at the surface of the sample.[3] Simultaneous colloidal probe AFM and reflection

© Author(s) 2022

interference contrast microscopy were successfully used to study the compression mechanics of polymer brushes with a force sensitivity of a typical AFM sensor, yet only with an absolute distance resolution of 2–3 nm, at best.[4] In addition, this technique is limited to macroscopic (optically resolvable) colloidal probe tips.

Complementarily, the SFA has been used for more than 40 years for the simultaneous, yet decoupled, measurement of surface forces and absolute positioning in the z-direction (with Å-accuracy) using Multiple Beam White Light Interferometry (MBI).[5–9] In addition, MBI also provides a direct and dynamic visualization of evolving contact geometries. In contrast to AFM, SFA offers absolute vertical separation measurement and dynamic control with an accuracy of 50 pm between two opposing interfaces.[6,9] However, with its macroscopic probe dimensions (centimeters), it lacks the lateral resolution of AFM. In addition, forces are measured with double cantilever springs with spring constants of typically 500–1000 N/m. Consequently, the force sensitivity is limited to several tens of nN and single molecule interactions and single bond breaking cannot be observed with SFA. Instead, SFA has been widely used to explore multiple hydrogen and hydrophobic binding formations in parallel[10–12] and various interfacial forces between opposing surfaces, including steric forces and structural forces due to confined fluid interfaces[12–14] in very close proximity (below 1 nm) and with Å-resolution.

Here, we developed a solution to this existing problem in terms of a unique experimental setup, which we call the Surface Forces Clamp (SFC). This setup is capable of nanometer control of the actual constraints, i.e., the surface and an SPM probe, over (in principle infinitely) extended timescales. The Surface Forces Clamp (SFC) provides the possibility for AFM-inspired measurement and control of surface forces. Simultaneously, SFA inspired MBI-based absolute distance control between the probe and the point of interest allows a unique measurement and control of sensor motions with sub-nm resolution of absolute distances. This novel SFC has the potential to form, monitor, and stress a single molecule or ligand/receptor bond on the molecular hook with sub-nanometer control of molecular distances.

II. METHODS AND MATERIALS

A. Chemicals and materials

HNO_3 p.A. was purchased from VWR and was diluted to the experimental pH values using Milli-Q water. Gold surfaces were prepared by thermal evaporation in a home-built physical vapor deposition system at a base pressure of 2×10^{-6} mbar. Samples for SFA experiments consisted of freshly cleaved ruby muscovite mica obtained from S&J Trading (NY, USA). The protocol for SFA surface preparations has been described in detail in previous work.[15] Briefly, sheets of uniformly thick single terraces were cleaved by hand. Afterward, they were PVD backside coated with 25 nm of silver (sample sheet) and 40 nm of silver (probe sheet) for effective reflection mode operation.[16] The thus way prepared back-silvered mica sheets were epoxy glued onto fused quartz disks with cylindrical curvature in a way the crystal lattice orientations of the sample and probe side were retained in a crossed cylinder orientation of the disks.

B. Force probing equipment and consumables

1. The surface forces clamp—SFC

We built the SFC inside a home-built noise cancellation box on a passively isolated optical table (B9090ACH, ThorLabs) to reduce the effect of environment vibrations as well as temperature fluctuations. The bulk of the device has been constructed from Invar™ and stainless steel. Motions are provided by a MadCityLabs Inc. T-115 piezo driven microscopy stage with aperture. For external distance sensing, we used an FPS3010 displacement laser interferometer using D4/F14 sensor heads (attocube, Germany).

2. Atomic force microscopy

A Cypher AFM (Asylum Research, Santa Barbara, CA) was used for calibrating the spring constant of cantilevers using the implemented thermal noise methods. Colloidal probe cantilevers were used (CP-CONT-Au-C, obtained from NanoAndMore, Germany) with spherical gold colloids of 5.5–9 μm diameter. The colloids act as a spacer between the reflecting mirrors for Multiple Beam White Light Interferometry. For enhancing interferometry intensities, the cantilevers were Ti/Au coated (5/50 nm) at the colloidal side.

C. Optical path

The internal distance sensing white light path for reflection geometry has been constructed from ThorLabs parts similar to a previous setup.[16] An Andor iXon electron multiplying charge-coupled device (EMCCD) camera on an Oxford Instruments Kymera KY193i spectrometer (grating: 1200 lines/mm) was used for white light interferometry. The top view path features a green bandpass filter (532 ± 2 nm, FL532-10, Thorlabs) and a CMOS camera (DCC1645C, Thorlabs).

D. Software

For alignment, experiment control, and logging, we used home-made programs written in LabView using supplied libraries from MadCityLabs and attocube. The proportional–integral–differential (PID) controller functionality uses "PID Advanced Autotuning" function from the National Instruments LabView 2017 Autopid library. Analysis of white light interferometry spectra has been conducted using SFA Explorer 3.5.2.[16] Scripts for simulation of spectra used the SFA Explorer internal multiple matrix method library.

E. Experimental procedures

Experiments for keeping constant positions at different distances [used for Figs. 3(b) and 3(c)] were conducted in air. Dynamic SFA experiments [used for Figs. 2 and 3(a)] were performed in 1 mM solution of nitric acid.

As surfaces, round microscopy coverslips coated with 5 nm Ti and 15 nm of gold were used (serving as the interferometer surface as well). "AFM-like" experiments (used for Fig. 5) were performed in 1 mM solution of nitric acid.

All measurements have been conducted overnight under remote control of the machine to reduce vibrations and temperature fluctuations.

The entrance slit of the spectrometer had an opening of 20 μm. The camera sensor was set to a 2×2 binning. For the static SFA experiment, the EMCCD camera was set to an exposure time of

© Author(s) 2022

0.2 s resulting in a cycle time of 0.213 01 s. All other measurements have been set to an exposure time of 0.198 06 s to maintain a cycle time of 0.2 s. Spectra were recorded as 16 bit grayscale TIFF. The wavelength window has been controlled on a per-line basis using a mercury vapor reference lamp. The PID controller has been parameterized with a constant term of 0.25, an integration time of 0.01 min, and no derivative term. The total spring constant on the SFA sample holder was measured to be 8860 N/m. The spring constant of the AFM cantilever was measured to be 243 pN/nm.

III. CONCEPT

In this work, we describe the working principle of a novel design for an absolute distance-based force measuring apparatus, for which we coined the name surface forces clamp. As discussed above, SPM suffers from thermal drift, which can be minimized but not eliminated by hardware design and post-processing software solutions. What is not achieved in state-of-the-art AFM is an absolute distance control between the sample surface and the scanning probe. This would, in principle, allow a real-time drift correction, that is, constant positioning of the sample and surface in space and time. Here, we chose a method-independent approach to enable constant distance operation of in principle all different SPM methods, while we focus on exemplarily showing applications for AFM and SFA. As shown in Fig. 1, we have chosen an approach based on laser-based interferometric sensing of the relative position of the probe and the sample surface with respect to each other. In previous work, a different laser-based approach was also developed by the Kurihara group,[17] where an interferometric bouncing from the back of a single surface is utilized to measure the relative placement of an intransparent sample surface. In comparison to this so-called twin-path SFA, we have designed an interferometric clamping between upper and lower sample mounts and demonstrate its intrinsic stability and applicability for both AFM and SFA measurements.

A. Design principle

In detail, the central idea is to measure the position of the sample and probe with respect to each other—in terms of an absolute distance—using laser-based interferometers as a "distance clamp." This fixes an external absolute distance Z, which can directly relate to the surface separation D. Figure 1 shows a sketch of the essential design features and working modes of the designed devices.

From the conceptual point of view, the SFC (see Fig. 1) features a generic home-built inverse reflection microscope-like setup with interchangeable sample holder concepts to implement different SPM techniques. A piezo driven xyz-stage with an aperture provides relative motion for a sample with respect to a static probe.

The novel and unique aspect of this apparatus consists of a synergistic combination of MBI measurement of the absolute distance (D) between the sample and probe and a fast distance clamping and drift correction using an IR-laser Fabry–Pérot interferometry-based approach. The clamping is accomplished by comparing the laser distance Z (see Fig. 1) to a user-defined setpoint Sp_z, while simultaneously a PID-controlled approach corrects the relative position of the sample and probe by moving the xyz-stage. Thereby, the regulated output position reflects the intended absolute position as well as any necessary compensations due to sample and/or surface

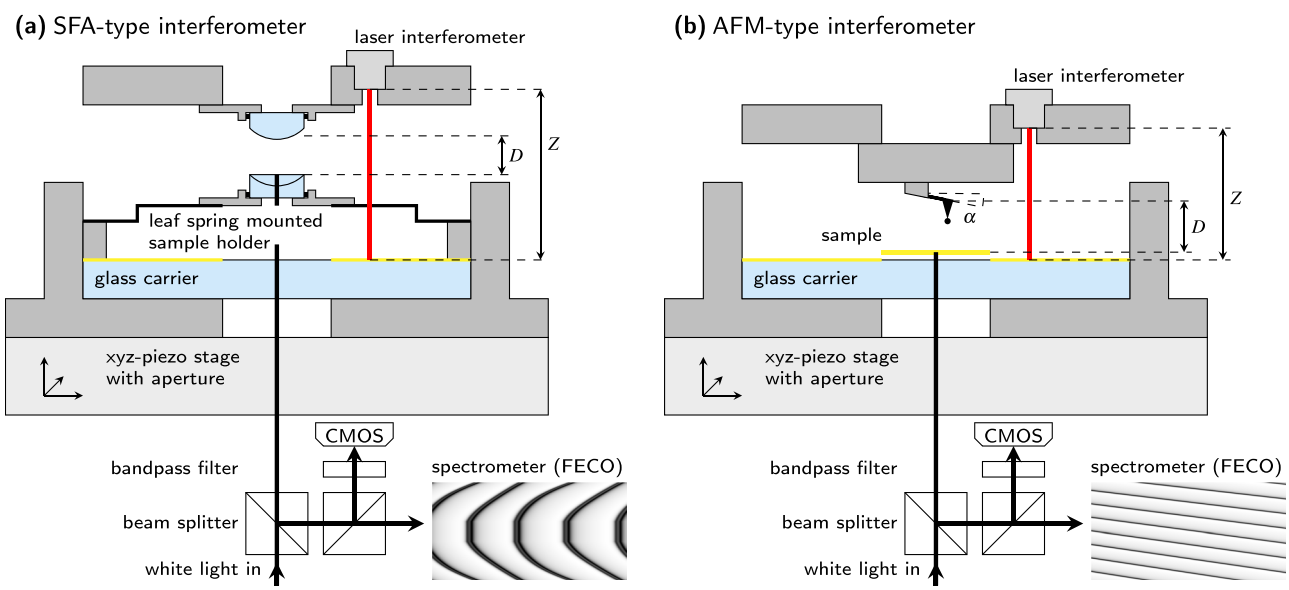

FIG. 1. Schematic drawing of the apparatus in SFA mode (a) and in AFM mode (b). Drift is measured using a Fabry–Pérot interferometer (laser interferometer) against the gold coated glass carrier (distance Z) and corrected using a PID-controlled xyz-piezo stage. The aperture in the piezo stage allows for measuring white light interferometry distances (distance D). In case white light interferometry is used, the emerging interference patterns can be analyzed as Fringes of Equal Chromatographic Order (FECO) after spectroscopic splitting (simulated patterns expected for both measurement modes depicted as insets) or as Newton rings [for example, see Fig. 5(a)] by using a bandpass filter and a CMOS camera. In the SFA mode (a), the interferometer is composed like a classical SFA-type crossed cylindrical quartz disk in mica–mica reflection geometry. For the AFM mode (b), the interferometer is built using a bottom-side gold coated colloidal probe AFM cantilever against a gold coated microscopy coverslip.

© Author(s) 2022

drift in the z-direction. These can then be fully compensated in real time with up to kHz reaction time given the currently utilized laser hardware.

Hence, the PID output (PID_z) position corrects for the intended absolute position of the sample and the probe holder with respect to each other, which includes drift correction as well as machine characteristics. In turn, Z characterizes the absolute sample to probe holder distance, which is the process variable of the PID loop. The FECO distance (D) reflects an absolute distance of the sample and probe measured by classical SFA in reflection mode geometry, which can also be used for benchmarking the absolute Z positioning quality. Furthermore, the difference between D and PID_z contains information about forces inherent to the samples used (e.g., surface forces).

Similar to the SFA approach, by a definition of the contact position, that is, when the sample and probe touch in a dry atmosphere, it is hence possible to set an absolute sample-to-probe distance using the IR-laser Fabry–Pérot interferometry approach for both the AFM- and the SFA-like setup.

IV. RESULTS AND DISCUSSION

In this section, we will discuss the newly constructed device in terms of benchmark experiments in both AFM and SFA mode operation.

A. SFA measurements and characterization of device behavior

First, Fig. 2(a) shows a comparison between setpoint (Sp_z) and PID_z positions, recorded during continuous open-loop (piezo not linearized by the closed-loop strain-gauge extension sensors) approach/separation. The recorded data show the expected sigmoidal deviation from an idealized linear response of the piezo for $Sp_z = PID_z$. Approach curves (circles) exhibit a slightly different dependence as compared to separations (triangles) indicating a typical hysteresis. This is the inherent piezo characteristic, as expected for an open-loop operation.

In our approach, the PID sensor directly corrects the piezo characteristic by utilizing the absolute distance derived from the Fabry–Pérot interferometer. In this sense, the interferometric distance acts as a sensor for linearizing the piezo characteristics during operation; that is, effectively setting up a closed-loop control with the laser-based distance sensor.

This closed-loop operation principle can now be directly benchmarked using an SFA-based force vs distance experiment. Therefore, we performed a force measurement between two mica surfaces (in crossed cylinder geometry) in HNO_3 at a pH of 3.0.

Figure 2(b) shows the linearized (corrected) PID_z position vs the distance D measured by the SFA approach. The data indicated a clear linear relation between D and PID_z. The white light interferometry measured distance D reflects the PID set position PID_z linearly with three exceptions, which are as follows: When (1) sample and probe touch in hard contact ($D = 0$, ‡), (2) at a distance of about 30–40 nm before close contact (long-distance forces), and (3) during separation where an adhesive jump out of contact (jump out) occurs due to the adhesive hysteresis (†).

These data can be further directly transformed into a force vs distance characteristic by subtracting the linear approach rate from the data shown in Fig. 2(b). As customary in SFA, forces have been calculated assuming this linear approach rate between PID_z and D values using the spring constant of the sample holder (8860 N/m in this case).

Figure 3 shows the resulting force vs distance characteristic. The force characteristics during approach and separation indicate a stable zero-force line for large separation distances up to 120 nm as well as the expected hard wall at very close separation distances of about 0.73 Å. The data indicate a typical approach curve expected

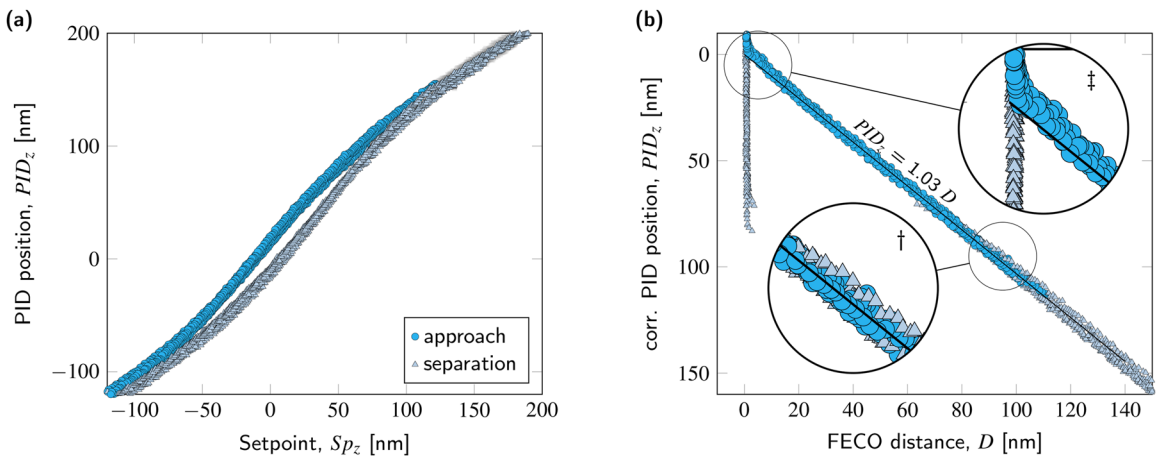

FIG. 2. In order to match the laser interferometric distance (Z) to a given setpoint (Sp_z), the stage is moved to a position determined by the PID controller (PID_z). (a) PID_z plotted against Sp_z shows a sigmoidal dependency and hysteresis (only one occurrence shown) originating from characteristics of a stack of piezo crystals used to drive the xyz-stage. (b) After correction for drift over time (offset shifted to match the other forceruns), PID_z in comparison with the FECO distance (D) shows further relaxations of the system at large distances (†) in addition to the expected deviations near contact (‡) caused by surface interaction forces. As a result, the overall slope is 1.03.

© Author(s) 2022

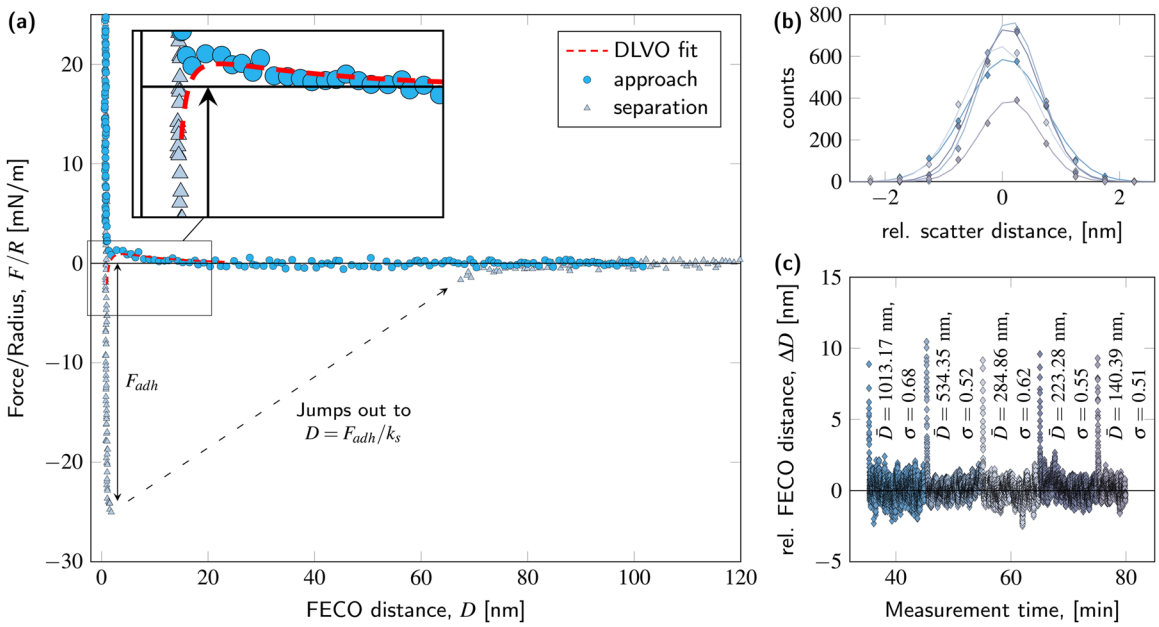

FIG. 3. (a) Force vs distance characteristic recorded during approach and separation of two mica surfaces in HNO_3 at pH = 3. (b) Histogram of the stabilized distance over 10 min (last distance over 5 min). (c) Recorded relative distance changes (ΔD) during stabilization of given distances over 10 min each (last distance over 5 min), respectively (see also text for details). For better visibility of the noise level, the average set distance of each step (denoted as $\bar{D}$) has been subtracted from the position data of that step. The apparent spikes indicate the motion during a jump between two set distances. The equilibration times depend on the jump distance and feedback settings and are in the range of a few seconds. Color codes of each step correspond to those in (b).

for two mica surfaces immersed in water at mildly acidic pH levels of 3.0 with an ionic strength of 1 mM.

The data can be fitted well using the DLVO theory (red dashed line) with literature and theoretical values[18] for the Hamaker constant (2.2×10^{-20} J) and the Debye length (9.61×10^{-9} m). The fitted interaction constant of 16.71×10^{-12} J/m, which corresponds to a surface potential of 47 mV, is in perfect agreement with expectations for mica vs mica, where the surface is already partially protonated, close to the point of zero charge between pH = 2–2.5.

For further characterizing drift compensation characteristics, a "set-and-hold" experiment, at given distances D, was performed. Therefore, a constant distance ramp with decreasing separation was programmed, at each step, the distance was stabilized by the Fabry–Pérot interferometry (constant distance clamping), and we recorded D for 10 min. This allows us to track and benchmark the absolute distance clamping capacity of the constructed device.

Figure 3(c) shows the deviation (ΔD) of the measured D from their distance average ($\bar{D}$) as a function of time and approach steps, respectively. It can be seen that the system stabilizes the absolute distance between the two surfaces well within 1 nm over an extended time of up to 10 min. In principle, this can be extended to any desired extended time period (in practice, as long as an experimental system will be stable).

Since the focus of this benchmark experiment is the long-time stability, the first 100 data points (20 s) of each step, during stabilization of D after the jump to the next set distance, were not taken into account for calculating averages as well as histograms (b).

This yields a Gaussian distributed absolute distance over this extended time period. Gaussian fits of the distance histograms are depicted in Fig. 3(b) with the standard deviation of each step shown in inset (c) (σ). These data demonstrate that D can be successfully stabilized to within 0.5–0.6 Å over 10 min. Virtually no significant drift occurred in this closed-loop system, which is stabilized by the implemented Fabry–Pérot distance clamping mechanism.

These results confirm and support that the laser-based interferometric distance clamping can be directly utilized as an absolute distance clamp. Precisely, the absolute position distance clamping was confirmed by MBI. Application of this setup can include, for instance, measurements between non-transparent samples, complex multilayered samples, or samples with gradients of refractive indices, where the absolute character of the MBI approach becomes limited by the modeling of the sample, or any other type of SPM methods. Here, we now focus on demonstrating that this mechanism can be utilized to also record *absolute* force vs distance characteristics in an AFM geometry.

B. MBI AFM theory and measurements

As shown in Fig. 1(b), we constructed a second sample holder for mounting a standard commercial AFM cantilever chip with a colloidal probe of a given radius of 5.5–9 μm, effectively forming an interferometric cavity of (gold | solution | gold). It is our aim to probe the piezo feedback regulation with the Fabry–Pèrot laser interferometer also for AFM while simultaneously evaluating the quality

© Author(s) 2022

of the distance readout with MBI directly from an interferometer constructed between the cantilever and surface.

This requires a reflection mode operation of the MBI, here with a gold cantilever (with a reflective 50 nm gold coating on the sample side) and a surface with a semi-transparent gold coating (15 nm).

For this first set of experiments, we chose a colloidal probe system due to geometric restriction of commercial cantilevers with fine needle tips. Specifically, commercially available AFM cantilevers are optimized for a mounting angle of 10° in order to allow for easy mounting as well as detection using the beam bouncing method. In addition, the tip height is usually about 15 μm, which sets a too large distance for highly resolved MBI. Due to its spherical geometry, and selectable size, a colloidal probe tip *per se* does not require any special angle mounting and provides a selected separation distance based on the colloidal radius. In principle, it is possible to perform the following experiments with needle tips as well.

Considering these cantilever limitations, MBI is further preferably performed with interacting surfaces normal to the propagation direction of the light used in detection. In practice, it is possible to go to a shallow angle of about 2°–3°, without the risk of touching the sample with the cantilever chip instead of the tip. This angle will, however, also influence the distance resolution with MBI as follows.

Figure 4(a) depicts the influence of the angle of the cantilever (α) on the expected spectral patterns of the signal in MBI based on a simulation for a 5° tilt of the cantilever.

First, and as expected, the propagating light waves of the incident light form a continuous distribution of interference patterns for each distance, as indicated in Fig. 4(b). However, the resolution on the detector is limited by the optical path, dispersion of the spectrometer, and the pixel size of the camera chip. Hence, with increasing tilt angle, an increasingly larger range of distances is smeared out onto one single pixel of the detector. As indicated in the figure panel (b), this results in an integral spectrum on each pixel.

These smeared interference patterns strongly depend on the distance distribution seen by each single camera pixel, and a lower angle will considerably increase the resolution.

In detail, Fig. 4(b) shows the simulation of a selection of those overlapping interference patterns emerging from 100 even-spaced distances convoluting on a single pixel given a mounting angle of 5° and the set total dispersion of our device as well as the resulting overlap spectrum at the bottom of the graph.

Figure 4(c) shows the comparison of overlap spectra (solid lines) to the respective single spectrum at median distance (dashed lines) for different mounting angles. The simulation shows not only a broadening of the destructive interference patterns (minima), but also a significant shift of the spectral position of the minima for higher angles. In any case, it is possible to simulate such patterns for any given tilt angle, providing a possibility to track Fringes of Equal Chromatographic Order (FECO) directly from an AFM cantilever.

Consequently, from an experimental point of view, it is ideal to lower the mounting angle as much as possible, given the currently available commercial cantilever chip design. Hence, actual experiments have subsequently been performed using a mounting angle of about 2.5°.

Figure 5 shows results of a force vs distance experiment also recorded in HNO_3 at a pH of 3. Several interesting aspects of this experiment can be summarized as follows.

First, panel (a) shows a series of patterns recorded during approach and increased compression in hard contact at $D = 0$. Indeed, reflection mode detection provides an expected Newton pattern for a cantilever beam in the top view camera (green notch filter with ±2 nm around 532 nm). At large separation (left), the pattern indicates lines of alternating increased and decreased intensity with shorter separations at larger distances. In hard contact, the pattern offers a direct view into the deformation of the cantilever beam. As can be seen, the top of the tip (contact point) remains at a stable distance, while the center of the beam starts to bend considerably,

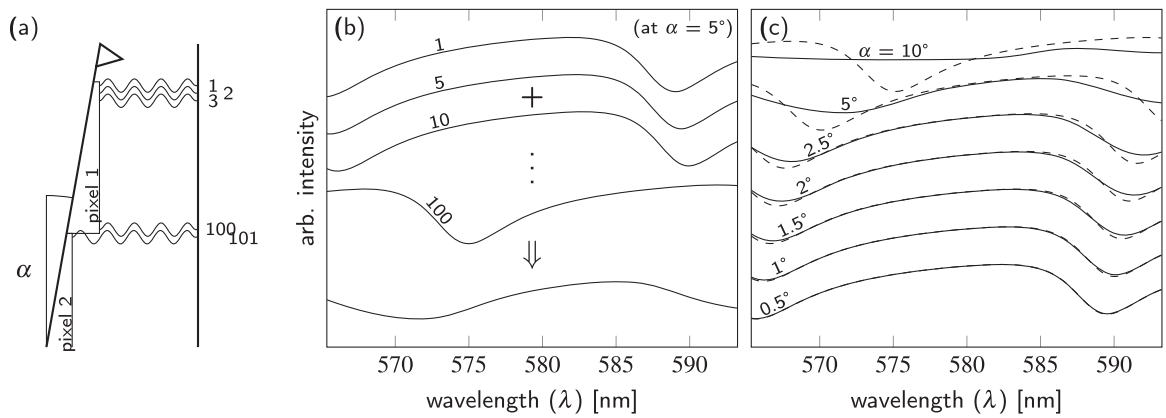

FIG. 4. Theoretical evaluation of the influence of the cantilever mounting angle (α) on white light interferometric spectra. (a) Interference patterns of different distances (denoted by a number, e.g., 1–101) between the cantilever and surface will occur on the same pixel on the detector camera. (b) The resulting superposition of those patterns (1–100) can cause peak broadening and loss of contrast; to an extent, line-based analysis is no longer usable. (c) Comparison of resolution-limited spectra at certain mounting angles α (solid lines) compared to the midpoint distance of the same distance interval (dashed lines) (simulations have been done for 100 distance steps per line in a spectrum at a lateral dispersion of 1107.595 nm/px).

© Author(s) 2022

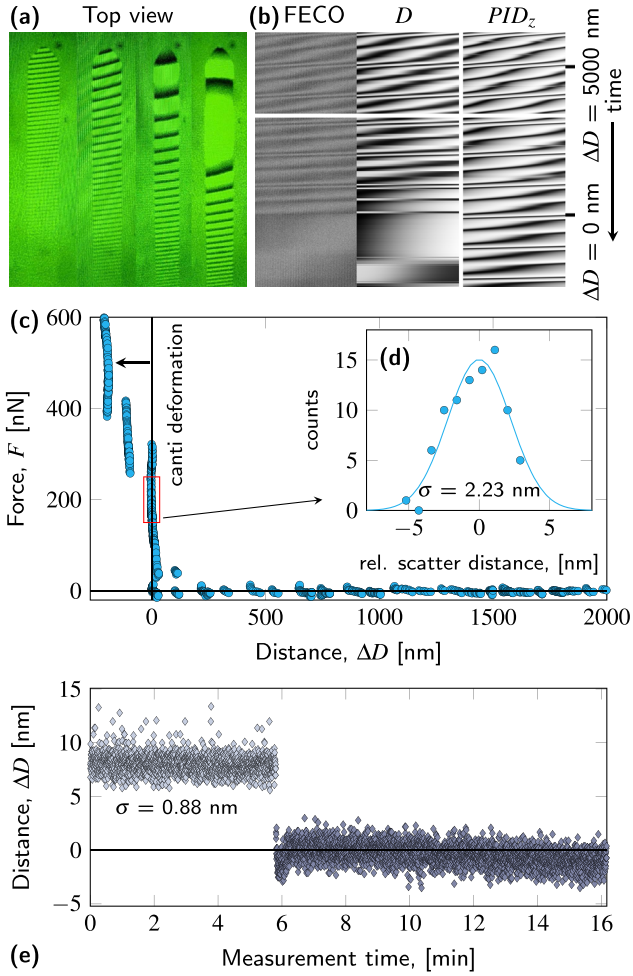

FIG. 5. (a) Newton ring pattern on the AFM cantilever as seen through the top view path, using a bandpass filter, at different distances between the cantilever and sample during compression. The third image is near contact, the forth compressing hard enough to bend the cantilever and force a "belly." (b) Spectra as seen in a time series during compression (from top to bottom, each line is one frame). Left (FECO): the measured spectra after background subtraction; middle and right: a simulation of spectra from the fitted distances (D) and the stage positions (PID_z). To keep consistency to common descriptions within the SFA community, the absolute distances (D) are referenced to the absolute distance in contact of probe and sample forming the distance ΔD. (c) Force/distance curve for this compression. Inset (d): histogram of the fitted distances during contact before deformation starts (red box) and Gaussian fit over the histogram. (e) Jump into contact from hovering at a stable distance of 8 nm.

as expected for a spring. Hence, Newton ring analysis provides a direct view of cantilever deformations *in situ*, to an extent that cannot be derived from the classical beam bouncing methods. This will be particularly useful for applications in tribology, where real-time deformation profiles of the tip are crucial for understanding sample/probe interactions.

Second, panel (b) shows a time series of FECO patterns, the simulated patterns for deriving the distance, as well as the PID signal (linear piezo approach) recorded/analyzed for an approach run at a typical AFM approach rate of 100 nm/s. Importantly, it is possible to capture FECO, directly from an approaching AFM cantilever, but the AFM approach rate is not ideal for FECO recording. Still, we aim for this comparison to compare first directly to a typical AFM force probe experiment.

It further has to be emphasized that the approach is controlled in feedback with the Fabry–Pérot distance clamping. As such, the comparison of the FECO pattern, the simulated pattern, and the PID pattern indicates a well regulated system also for an AFM force probe experiment. These data uniquely confirm that it is possible to utilize MBI even for an AFM geometry, which immediately makes AFM an absolute distance controllable technology, similar to SFA. Excitingly, it is now possible to translate the measured FECO distances into a force vs distance characteristic similar to SFA.

Panel (c) shows the derived force vs distance characteristic. While rather noisy, due to the typical and fast AFM approach rate, the data demonstrate a clear and absolute distance regulated approach from a 2000 μm distance. As expected, the sample touches the surface and runs into a hard wall at $D = 0$. No standard correction for the cantilever bending[1] had to be applied to derive a true distance vs force pattern for an AFM force probe experiment. The zero distance can be defined similar to an SFA approach based on a (dry) reference measurement. Once a proper zero distance is defined, any distance can be referred to this reference in terms of an absolute distance.

As such, this provides an absolute force vs distance, and the possibility to set any distance in future experiments using FECO and/or the Fabry–Pérot distance clamp. In hard contact, when the sample/tip separation does not change significantly, the resolution of the MBI can be read out from a Gaussian distribution of the measured distance. As can be seen in the inset (d), we can currently achieve an absolute distance resolution of about ±2–3 nm. This is about a factor of 2–3 better compared to an absolute distance sensing using reflection interference microscopy on a colloidal probe.[4,19,20] One should further keep in mind that the applied load still changes with a ramp rate of 100 nm/s. Hence, this is a lower limit of the distance resolution under non-ideal conditions for MBI.

Furthermore, from the zero-force line, it is possible to read out a force resolution, which is about ±5–10 nN with the applied system settings (rate of approach, etc.). Again, this is the lower limit of any resolution at the typical AFM approach rate. As a side note, and as can also be seen, during highest compression, we see apparent distance jumps in hard contact. We attribute these to sliding and resulting deformation changes of the cantilever, or possibly even indentation events. A further analysis of such events is out of the scope of this work, but will be considered in future work with the system.

We now further demonstrate what is possible with the absolute distance capacity, and we evaluate the possible force and distance resolution of this approach, when we conducted an AFM experiment in a quasistatic approach. Figure 5(e) shows again a "set-and-hold" experiment. In detail, we aim to fix the AFM cantilever distance using the Fabry–Pérot interferometer. We verify the stable distance by recording the absolute distance using MBI. The figure shows how an AFM cantilever hovers at a stable distance of 8 nm over the probe surface for 5 min. Afterward, the piezo jumps into contact and applies a constant load. This demonstrates that any drift

© Author(s) 2022

and other non-linearities of the system were eliminated successfully by the laser-based PID controls. The distance noise during hovering is ~0.9 nm (RMS) without any oversampling. As expected, this is better, approximately by a factor of three, compared to the fast approach rate at 100 nm/s shown in panel (c).

From this experiment, we can further estimate the force resolution of the system when used in the MBI mode. In such a mode, the force is limited by the distance resolution, as forces are measured as deviation from applied approach distances (as in classical SFA). Based on Hook's law, we can estimate that the smallest measurable force is hence $F_{\min} = k\Delta D$. With a typical AFM cantilever force constant of 0.08 N/m and a distance resolution of 0.9 nm, this translates into a theoretical force resolution of 60–80 pN, without oversampling. This is in the range of the classical AFM measurement.

C. Complementary discussion of force probe techniques and the SFC principle

In summary, we demonstrated two important aspects with implication for force probe experiments.

First, a Fabry–Pérot absolute distance clamping is capable of stabilizing an SPM and SFA device. Furthermore, the absolute Fabry–Pèrot distance can be utilized as a feedback regulation parameter for SFA as well as AFM experiments. We want to emphasize that the clamping in itself is independent of the technique that it is used with. In addition, during application, it will not be necessary to measure MBI simultaneously; here, we used it to demonstrate the absolute distance clamping. In essence, it was necessary to prove the principle. Given the expected force and distance resolution, MBI will be a useful add-on for classical AFM, and it also provides a direct 3D and real-time view of cantilever deformations.

As such, our system provides an indirect distance clamping, which perfectly correlates with the absolute distance measurement by MBI demonstrated by direct comparison to the SFA approach. The distance clamp is an ideal and fast method for stabilizing the probe to sample relation, irrespective of the application. Here, we demonstrated AFM and SFA applications, but, in principle, any relation of a probe to a sample can be fixed by this approach. In the field of SPM, this will allow us now to conduct distance stabilized force probe experiments with nanometer lateral resolution. In a classical SFA, the resolution is limited to a few micrometers.

Furthermore, and this is the second point, we also demonstrated MBI at the sub-nm resolution directly from an AFM cantilever. In this work, we could prove the principle and show that one can generate and analyze FECO data from direct cantilever bouncing. This enables true and directly measured force vs distance relations in AFM. Here, we want to emphasize again how this deviates from traditional setting of a probe–sample distance in an AFM. In fact, a traditional AFM does not measure any distance. Instead, it moves the cantilever against a surface, and only controls the voltage applied to a piezo, while measuring a cantilever deflection. At any distance away from contact, the deflection is zero, irrespective of the distance. Hence, no direct distance information is available. Only when the surface is touched, which is when the cantilever deflects, the extension of the piezo can be related to a distance from the surfaces. As such, this is an *a posteriori* referencing. Given that the AFM drifts thermally, any reference looses validity after a short amount of time. Furthermore, a closed-loop scanner in AFM also does not measure any probe–sample distance. Instead, it measures the length of a piezo, by which it regulates to the desired value. If there were no drift, this would be also an absolute reference frame, but this is not the case. Therefore, our approach, while complex and seemingly complicated and too tedious for a standard AFM, truly enables the measurement and feedback regulation with a distance measure between the probe and the sample, especially a true absolute distance. This allows for new experiments with new feedback variables.

Under optimized conditions (quasistatic measurement at a fixed distance), the distance readout from the MBI is ±0.9 nm, which correlates with a force resolution of 60–80 pN depending on the cantilever used. This is in the single molecular range and will hence allow us to make use of SFA advantages at the AFM-enabled nanoscale. If it is possible to reach the full SFA distance accuracy of ±0.1 nm, the best expected force resolution will be around 5–20 pN. This will reach the limits of classical beam bouncing AFM, but at absolute distance control, enabling completely new SFA-like force probe experiments at the nanoscale. Should this not be possible, it is always possible to combine the distance clamping with a traditional beam bouncing readout. This may become useful, considering that FECO readout (at up to 100 fps) is also considerably slower compared to beam bouncing in the 2–5 kHz sampling range.

V. CONCLUSION

In this work, we developed a novel absolute position control for force probe experiments. The device utilizes a feedback-regulated laser interferometer for stabilizing the absolute distance between the probe and the sample surface. We demonstrated the capabilities of this interferometrically stabilized scanning probe device using benchmark experiments and comparison to AFM and SFA operation modes. In detail, we demonstrated that

- The absolute positioning is accurate to within 0.6 ± 0.2 nm RMS deviation of the distance between the sample and probe, irrespective of the operation mode (AFM/SFA).
- Absolute position can be held with the same accuracy over extended time scales (we tested up to 10 min).
- Data output from the SFA operation mode is directly comparable to traditional SFA. However, in comparison to fastest acquisition rates of traditional SFA (max. 50–100 Hz), this setup now allows a feedback-regulated absolute distance control with up to several kHz (comparable to AFM).
- In principle, the device allows for SFA-like experiments with non-transparent surfaces and complex surfaces.
- Direct white light interferometry in reflection mode is possible with AFM cantilevers. Signals are weak, yet well detectable and analyzable. The absolute distance accuracy with FECO analysis is currently limited to about ±3 nm, with potential for further improvement based on increased signal to noise ratios.
- Newton patterns provide a direct visualization of the AFM cantilever bending, providing a 3D real-time view of torsions during the experiment.

In summary, with this new setup, it is possible to perform distance controlled experiments for both AFM and SFA setups and over

© Author(s) 2022

extended time scales (>10 min). This will enable, for example, equilibrium force probing with AFM, probing of fluctuating two-state systems (protein interaction imaging), as well as constant distance and force probing of electrochemical modulations in confinement with the SFA. In addition, it is possible to extend the concept to 3D to enable constant distance positioning with single molecular accuracy in all three spatial dimensions. In the AFM mode, imaging the cantilever bending *in situ* may provide important insight into nano-friction experiments, local compressibility of thin films and solid electrolyte interfaces, and with new cantilever designs, higher accuracy may become possible. Hence, the developed new technology will prove useful for scanning probe microscopy in general, and it will allow new measurement modes, which are to date not possible. The described advances can possibly be retrofit to some existing system designs.

ACKNOWLEDGMENTS

We acknowledge support by the European Research Council (Grant No. CSI.interface, ERC-StG 677663) as well as the Max-Planck Institut für Eisenforschung. We are grateful to Dominik Dworschak for determining the force constant of our AFM cantilevers.

AUTHOR DECLARATIONS

Conflict of Interest

The authors have no conflicts to disclose.

Author Contributions

Kai A. Schwenzfeier: Conceptualization (supporting); Software (lead); Validation (lead); Visualization (lead); Writing – original draft (equal); Writing – review & editing (equal). **Markus Valtiner:** Conceptualization (lead); Investigation (lead); Project administration (lead); Resources (lead); Supervision (lead); Writing – original draft (equal); Writing – review & editing (equal).

DATA AVAILABILITY

The data that support the findings of this study are available from the corresponding author upon reasonable request.

REFERENCES

[1] H.-J. Butt, B. Cappella, and M. Kappl, "Force measurements with the atomic force microscope: Technique, interpretation and applications," Surf. Sci. Rep. **59**, 1–152 (2005).
[2] G. M. King, A. R. Carter, A. B. Churnside, L. S. Eberle, and T. T. Perkins, "Ultrastable atomic force microscopy: Atomic-scale stability and registration in ambient conditions," Nano Lett. **9**, 1451–1456 (2009).
[3] C. T. McKee, W. K. J. Mosse, and W. A. Ducker, "Measurement of the absolute separation for atomic force microscopy measurements in the presence of adsorbed polymer," Rev. Sci. Instrum. **77**, 053706 (2006).
[4] S. Attili and R. P. Richter, "Combining colloidal probe atomic force and reflection interference contrast microscopy to study the compressive mechanics of hyaluronan brushes," Langmuir **28**, 3206–3216 (2012).
[5] J. N. Israelachvili, "Thin film studies using multiple-beam interferometry," J. Colloid Interface Sci. **44**, 259–272 (1973).
[6] J. Israelachvili and D. Gourdon, "Putting liquids under molecular-scale confinement," Science **292**, 867–868 (2001).
[7] J. N. Israelachvili, Y. Min, M. Akbulut, A. Alig, G. Carver, W. Greene, K. Kristiansen, E. Meyer, N. Pesika, K. Rosenberg, and H. Zeng, "Recent advances in the surface forces apparatus (SFA) technique," Rep. Prog. Phys. **73**, 036601 (2010).
[8] J. N. Israelachvili and D. Tabor, "Measurement of van der Waals dispersion forces in range 1.4 to 130 nm," Nat. Phys. Sci. **236**, 106 (1972).
[9] B. R. Shrestha, T. Baimpos, S. Raman, and M. Valtiner, "Angstrom-resolved real-time dissection of electrochemically active noble metal interfaces," ACS Nano **8**, 5979–5987 (2014).
[10] J. Israelachvili and R. Pashley, "The hydrophobic interaction is long-range, decaying exponentially with distance," Nature **300**, 341–342 (1982).
[11] J. N. Isrealachvili and R. M. Pashley, "Molecular layering of water at surfaces and origin of repulsive hydration forces," Nature **306**, 249–250 (1983).
[12] M. Valtiner, S. H. Donaldson, Jr., M. A. Gebbie, and J. N. Israelachvili, "Hydrophobic forces, electrostatic steering, and acid–base bridging between atomically smooth self-assembled monolayers and end-functionalized PEGolated lipid bilayers," J. Am. Chem. Soc. **134**, 1746–1753 (2012).
[13] R. Gupta and J. Fréchette, "Interferometry of surfaces with well-defined topography in the surface force apparatus," J. Colloid Interface Sci. **412**, 82–88 (2013).
[14] M. Valtiner, X. Banquy, K. Kristiansen, G. W. Greene, and J. N. Israelachvili, "The electrochemical surface forces apparatus: The effect of surface roughness, electrostatic surface potentials, and anodic oxide growth on interaction forces, and friction between dissimilar surfaces in aqueous solutions," Langmuir **28**, 13080–13093 (2012).
[15] J. N. Israelachvili, N. A. Alcantar, N. Maeda, T. E. Mates, and M. Ruths, "Preparing contamination-free mica substrates for surface characterization, force measurements, and imaging," Langmuir **20**, 3616–3622 (2004).
[16] K. A. Schwenzfeier, A. Erbe, P. Bilotto, M. Lengauer, C. Merola, H.-W. Cheng, L. L. E. Mears, and M. Valtiner, "Optimizing multiple beam interferometry in the surface forces apparatus: Novel optics, reflection mode modeling, metal layer thicknesses, birefringence, and rotation of anisotropic layers," Rev. Sci. Instrum. **90**, 043908 (2019).
[17] S. Fujii, M. Kasuya, and K. Kurihara, "Characterization of platinum electrode surfaces by electrochemical surface forces measurement," J. Phys. Chem. C **121**, 26406–26413 (2017).
[18] J. N. Israelachvili, *Intermolecular and Surface Forces* (Elsevier, Academic Press, 2011).
[19] P. E. Hillner, M. Radmacher, and P. K. Hansma, "Combined atomic force and scanning reflection interference contrast microscopy," Scanning **17**, 144–147 (1995).
[20] J. K. Stuart and V. Hlady, "Reflection interference contrast microscopy combined with scanning force microscopy verifies the nature of protein–ligand interaction force measurements," Biophys. J. **76**, 500 (1999).

© Author(s) 2022